

Hybrid method for modeling epitaxial growth: Kinetic Monte Carlo plus molecular dynamics

P. Zoontjens,¹ T. P. Schulze,² and S. C. Hendy^{1,3}

¹*MacDiarmid Institute for Advanced Materials and Nanotechnology, School of Chemical and Physical Sciences, Victoria University of Wellington, Wellington 6140, New Zealand*

²*Department of Mathematics, University of Tennessee, Knoxville, Tennessee 37996-1300, USA*

³*Industrial Research Ltd., Lower Hutt 5040, New Zealand*

(Received 12 August 2007; published 18 December 2007)

We propose a concurrently coupled hybrid molecular dynamics (MD) and kinetic Monte Carlo (KMC) algorithm to simulate the motion of grain boundaries between fcc and hcp islands during epitaxial growth on a fcc (111) surface. The method combines MD and KMC in an adaptive spatial domain decomposition, so that near the grain boundary, atoms are treated using MD but away from the boundary atoms are simulated by KMC. The method allows the grain boundary to interact with structures that form on spatial scales significantly larger than that of the MD domain but with a negligible increase in computational cost.

DOI: [10.1103/PhysRevB.76.245418](https://doi.org/10.1103/PhysRevB.76.245418)

PACS number(s): 81.15.Aa, 02.70.Ns

I. INTRODUCTION

Epitaxial growth of thin films involves a number of disparate length and time scales, posing an enormous challenge for modeling and simulation.^{1,2} A popular and powerful approach to the simulation of such processes is the kinetic Monte Carlo (KMC) method (for a recent review, see Ref. 3), especially when combined with first principles determination of rates.⁴ While the standard KMC method assumes that atoms reside on a perfect lattice, this approximation is not always appropriate. For instance, both homoepitaxial⁵ or heteroepitaxial⁶ growth on a fcc (111) surface can lead to the formation of both fcc and hcp islands and the subsequent formation of grain boundaries as these islands impinge on one another.⁷ The mobility of grain boundaries is an important factor in determining the quality of thin films,⁸ and in several known instances, the mobility can depend on the interaction of the grain boundary with subsequent overlayer growth.^{6,9} However, such boundaries and other defects may be poorly described by the usual lattice approximation favored by standard KMC.¹⁰

Molecular dynamics (MD), on the other hand, does not rely on a lattice approximation. With an appropriate potential energy function, one would expect MD to give an accurate description of the structure and dynamics of a grain boundary or dislocation. However, the drawbacks of the conventional MD method include the need to compute forces between each pair of atoms in the simulation cell at each time step and an upper limit on the time step that can be taken to obtain a good solution to the corresponding equations of motion. In practice, this means that with MD, one can only simulate a relatively small number of atoms for relatively short durations. While this has motivated the development of a number accelerated MD algorithms which extend the time step (for a review, see Ref. 11), this remains a significant problem for the simulation of epitaxial growth, where the time scales involved generally prohibit the use of MD except in the limits of high temperatures and high deposition rates.¹²

Of course, this is a more general problem that has become particularly acute as interest in nanostructures intensifies. Although a nanostructure may consist of fewer atoms than its

micro- or macroscale counterpart, in many ways, it is less amenable to treatment by MD. Not only may it contain too many atoms to be feasibly simulated by MD, it will almost certainly lack the homogeneity of a larger system, preventing the use of a smaller simulation cell with periodic boundary conditions. These problems have motivated the development of hybrid multiscale methods which attempt to combine faster coarse-grained methods with atomistic simulation techniques (for a recent review, see Ref. 13).

Here, we present an algorithm that combines MD and KMC in an adaptive spatial domain decomposition in an attempt to reduce the computational cost of MD. We have used this method to study the motion of grain boundaries during epitaxial growth. Near the grain boundaries, atoms are treated using MD, but away from the boundaries, we use KMC. We note that Pomeroy *et al.*¹⁵ have described a scheme for hybrid MD-KMC. Their scheme involved consecutive application of MD and KMC to a single region rather than the concurrent, spatially decomposed adaptive algorithm we propose here. Several other hybrid schemes have been developed for modeling epitaxial growth based on spatial decomposition, including an algorithm that couples the continuum Burton-Cabrera-Frank (BCF) model to KMC.^{16,17} In principle, it would be possible to combine several such hybrid schemes with the method described here. We also note that it would be straightforward to utilize an accelerated MD method in our approach in place of the standard MD method used for illustrative purposes here.

II. METHODOLOGY

In our approach, the full system is evolved by performing one KMC step that moves the system time forward by an increment t_n .¹⁴ The rate for a KMC event depends on the location of neighboring MD and KMC atoms, and similarly, the MD atoms feel forces from the frozen KMC atoms up to the cutoff distance of the potential. To ensure that each domain interacts with a contemporaneous version of the other, the evolution of the KMC and MD regions should remain as synchronous as possible. Thus, the MD simulation is run for $t_n/\delta t$ steps (where δt is the MD time step) to catch up with

the KMC clock, although, in practice, one may select a number of KMC events to ensure that a minimum number of MD steps are performed (e.g., when the KMC region is much larger than the MD region, one might select multiple KMC events to ensure that $\sum t_n > \delta t$). At the end of such an iteration, the atoms are repartitioned into KMC and MD categories using an appropriate adaptive criteria. In the example studied below, the domain decomposition is adapted to follow the position of the grain boundary. One could consider a variety of other adaptive criteria, such as a threshold of strain induced by the grain boundary, for instance. Our choice here, which is based on distance from the position of the grain boundary, is perhaps the simplest and easiest to implement, although it is likely that more efficient schemes could be devised.

The reduced computational cost of the hybrid MD-KMC algorithm comes largely from avoiding the computation of forces between pairs of KMC atoms. If the system is described by a short-range potential with a cutoff, then the MD force calculation (accelerated or otherwise) would ordinarily scale as $O(N)$, where N is the total number of atoms. In this case, a domain decomposition with distinct KMC regions that are significantly larger than the potential cutoff will maximize the number of pairs of KMC atoms that can be ignored in the force calculation. This is the approach we adopt here, with distinct MD and KMC domains, reducing the computational time by a factor proportional to M/N , where M is the number of atoms in the MD domain(s). We note that one would also achieve a similar reduction in computational cost in a system with long range forces when an $O(N^2)$ force calculation is performed.

There are several artifacts that may arise at the interface between the MD and KMC domains. The first involves the reflection of phonons from the rigid atoms in the KMC lattice. This problem also arises in hybrid MD-continuum methods, and several techniques have now been proposed to deal with this issue.^{18,19} Secondly, we note that the rigidity of the KMC region, which in effect imposes a constant volume constraint on the MD region, will lead to stresses that may alter the mobility of atoms in the MD region. As the primary object of interest in this study is the migration of grain boundaries, we have dealt with these artifacts by (i) applying a Langevin thermostat²⁰ to the atoms in the MD regions to damp the reflection of phonons and to keep the MD atoms in thermal equilibrium and (ii) increasing the widths of the MD regions until we observed the convergence of the grain boundary diffusion coefficient.

III. APPLICATION TO GRAIN BOUNDARY MIGRATION

To illustrate the method, we will follow the propagation of a grain boundary between fcc and hcp islands nucleating on a fcc (111) surface by adaptively partitioning the system so that the grain boundaries are contained in MD regions as shown in Fig. 1. We first examine this system in the absence of adatom deposition. The types of boundaries that form between fcc and hcp islands are discussed in some detail in Ref. 7, and our simulations show both types of boundaries (A gaps and B gaps separated by kinks) described there. We

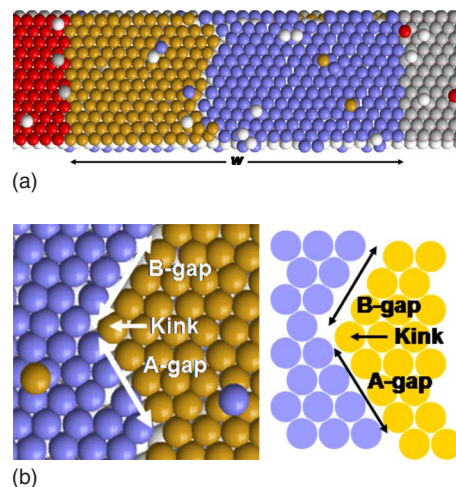


FIG. 1. (Color online) (Top) Snapshots showing the (instantaneous) decomposition of the system into KMC domains (far left and far right) and a MD domain (center) of width w , centered on a grain boundary. The atoms on the right occupy fcc sites, while the atoms on the left occupy hcp sites. (Bottom) A snapshot and a schematic representation of a typical grain boundary configuration showing a mixture of A- and B-type boundaries and a kink site where they meet.

have used our method to look at the mobility of such boundaries in the absence (this section) and presence of adatoms (next section). The Lennard-Jones potential (parametrized by the usual energy scale ϵ and length scale σ) with a cutoff of 3σ was used to calculate forces between MD atoms and forces between MD and KMC atoms. The nudged elastic band (NEB) method²¹ was used to determine energy barriers from this potential. However, in the absence of adatoms on the surface, there are no KMC events, so in this section the KMC will play no role in system evolution.

Figure 2 shows the results of several simulations using the adaptive domain decomposition algorithm without KMC events where we have plotted a time series of $x(t)$ defined as the instantaneous boundary position averaged across the short slab direction at a temperature of $0.3\epsilon/k_B$. The (111)-terminated slab used in the simulations was 6 atoms deep, 12 wide, and (at least) 72 long. Atoms in the KMC regions remain fixed on the lattice unless the boundary migrates, in which case, at the end of each interval t_n , the adaptive domain decomposition converts these regions to MD regions to keep the MD region centered on $x(t)$, the instantaneous position of the grain boundary. Atoms in the bottom layer of the MD region were also fixed. Here, we have chosen $t_n = 1\tau [=1\sigma(m/\epsilon)^{1/2}]$ in the absence any KMC rates.

Using this approach, we have examined the dependence of grain boundary migration on the width of the MD partition. Also in Fig. 2 we plot the time averaged square displacement $\Delta x^2 = [x(t+\Delta t) - x(t)]^2$ of the grain boundary position in a time interval Δt versus Δt for a variety of MD domain widths w , including a full MD simulation without partitioning. For each domain size, we collected data from 30 independent simulations (each of duration $10^4\tau$) to compute the curves seen in Fig. 2. As Δx^2 grows linearly with Δt , we

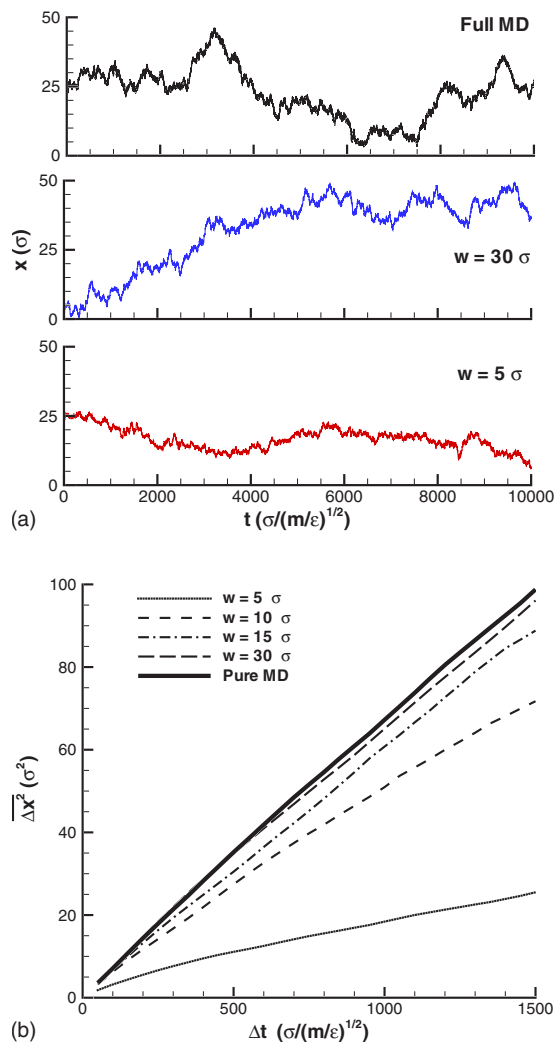


FIG. 2. (Color online) (Top) Evolution of the grain boundary position (defined as the average position of the boundary across the short direction of the slab) during typical simulations using the full MD method, the hybrid method with $w=30\sigma$, and the hybrid method with $w=5\sigma$. The mobility of the boundary in the $w=5\sigma$ MD domain is clearly suppressed. (Bottom) The mean square displacement $\overline{\Delta x^2}$ versus Δt for the full MD simulation and for the hybrid method for various MD domain sizes.

conclude that the grain boundaries are undergoing a diffusive random walk. We also observe a preference for hcp over fcc at this temperature, although this drift is generally not appreciable over the duration of a typical simulation. Note the convergence of $\overline{\Delta x^2}$ in Fig. 2 to that of the full MD result as the width of the MD regions increases, indicating that the dynamics of the boundary is no longer affected by the presence of the adaptive domain decomposition for sufficiently large w . Indeed, at $w=30\sigma$, we find that both the diffusive dynamics and the drift of the boundary are reproduced well by the hybrid method.

Using a domain decomposition with the width of the MD region $w=30\sigma$, we have undertaken further simulations of grain boundary migration over a range of temperatures, allowing us to identify the rate limiting step in boundary diffusion. Figure 3 shows an Arrhenius plot of the boundary

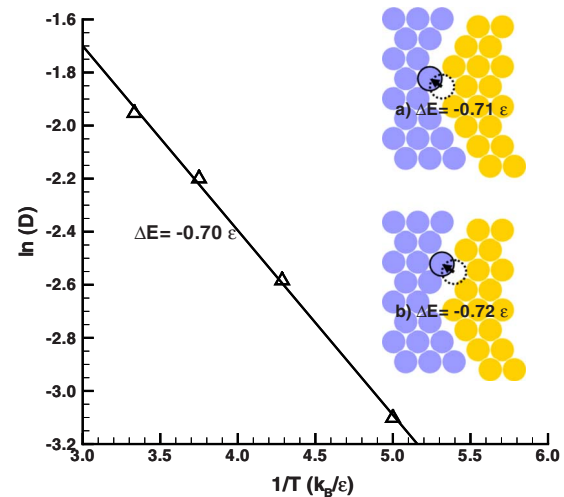


FIG. 3. (Color online) The dependence of the logarithm of the grain boundary diffusion coefficient D on temperature, calculated using the hybrid method. The slope of the plot gives an energy barrier $\Delta E=0.70\epsilon$. As expected, this is very close to the barriers for kink migration (shown in the inset are the important hcp to fcc kink migration steps), calculated using the NEB method, which limits the diffusion of the boundaries.

diffusion coefficient $D=\overline{\Delta x^2}/(2\Delta t)$, i.e., $\ln D$ vs $1/T$. The slope of the curve gives the energy barrier, $\Delta E=0.70\epsilon$, which presumably corresponds to that of the rate limiting step in grain boundary diffusion. As expected, this is very close to the NEB calculated energy barrier for kink migration, $\Delta E=(0.71\pm 0.01)\epsilon$, shown as the inset of Fig. 3. We note that with the cutoff used here, the NEB calculations reveal a slight 0.01ϵ preference for kink migration from fcc to hcp sites. Although this is consistent with the observed drift, it is a rather small preference which will be dominated by thermal effects at the temperatures examined here.

We note that as the boundary is constrained by periodic boundary conditions across the short slab direction, the boundary cannot develop significant curvature during propagation. Any curvature that does develop as the result of fluctuations will tend to drive the boundary back to its flat configuration producing no net drift. Indeed, we observe an average spread of the boundary in the long slab direction of only 2.8σ (the snapshot of the boundary in Fig. 1), which is close to atomic scale roughness. Nonetheless, we expect that the boundary mobility will depend on the slab width as it will affect the kink density along the boundary. These effects could be studied further using a wider slab which would be most efficiently handled by a more elaborate two-dimensional domain decomposition.

The mechanisms by which the rigid KMC region restricts the mobility of the boundary are not immediately apparent. As noted earlier, the rigid KMC region effectively imposes a constant volume constraint on the MD region which will cause corresponding stresses on this region. To examine this more systematically, we have computed a series of energy barriers for kink migration as a grain boundary approaches a rigid KMC boundary. The results are shown in Fig. 4. When the kink approaches within 2σ of the boundary, we can see

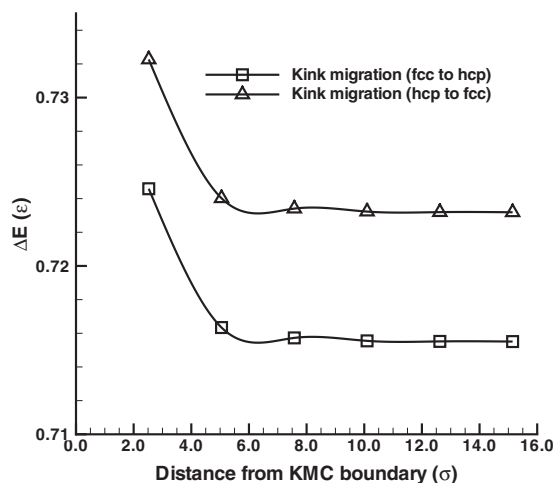
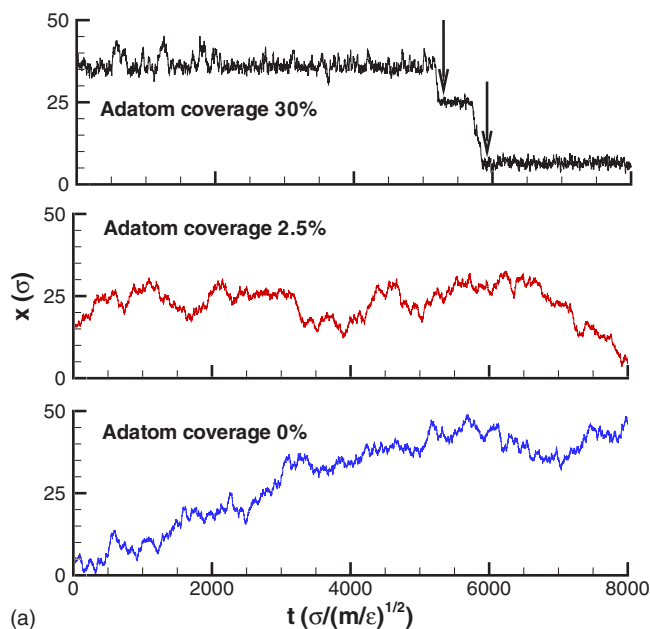


FIG. 4. The figure illustrates the change in energy barrier as calculated by the NEB method for a kink migration step as a function of the distance between kink site and the rigid KMC boundary.

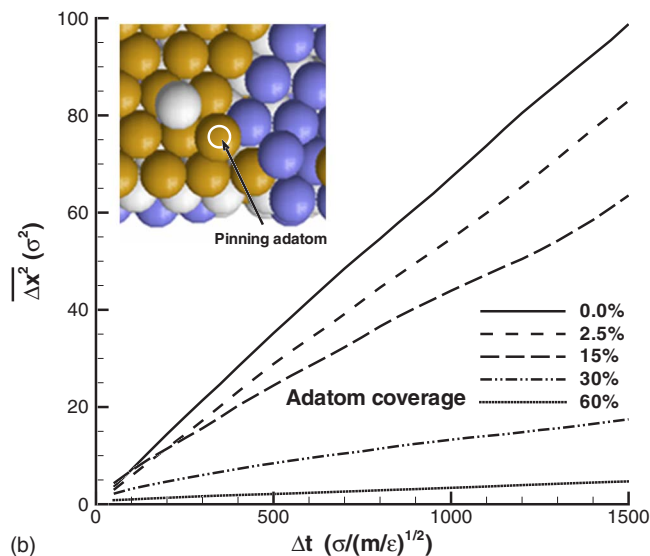
that the energy barrier increases by 0.01ϵ with no significant change in the hcp-fcc bias. This increase in barrier heights is to be expected as rigid atoms will not relax as the kink approaches. However, this effect is too small to fully explain the observed decrease in boundary mobility as the width of the MD region decreases (which we estimate is equivalent to an increase in barrier height of approximately 0.1ϵ when the size of the MD region is halved from 30σ to 15σ). Thus, it seems likely that the stresses due to the constant volume constraint have a stronger effect on the diffusion prefactor than the energy barriers. This also suggests that the efficiency of the method could be improved by relaxing the atoms in the KMC region to reduce the induced stresses and/or by using a domain decomposition based on strain rather than distance to the grain boundary. This will be explored in future work.

IV. GRAIN BOUNDARY MIGRATION WITH ADATOM DEPOSITION

To demonstrate the full hybrid scheme, we have investigated the effect of adatoms on the grain boundary mobility using a simple solid-on-solid-type KMC model for adatom diffusion on a (111)-terminated fcc surface, where energy barriers are a linear function of coordination number n , i.e., $\Delta E = E_n n + E_s$. While more complex models are available (e.g., Ref. 22), the simplicity of this approach is attractive for a hybrid scheme. We note that a similar approach has recently been used for modeling the evolution of fcc clusters toward their equilibrium shapes.²³ In addition, we use the rule that atoms can only move to, or be deposited on, sites that are unoccupied, are supported by a triad of nearest-neighbor atoms in the previous layer of growth, and have unoccupied neighboring sites. The second rule restricts in-plane moves to a subset of the six neighboring lattice sites. The last rule ensures that atoms do not overlap, as the lattice is the union of fcc and hcp lattices and the distance between neighboring sites is less than the nearest-neighbor distance in



(a)



(b)

FIG. 5. (Color online) (Top) Time series showing the movement of grain boundaries at different adatom coverages (0%, 2.5%, and 30%, respectively). At 30% coverage, the boundaries are generally pinned by adatoms and adatom islands, although motion can occur when the boundaries pass under islands (two such events are noted by arrows). At 2.5%, the pinning is generally not observed, although mobility is reduced as the boundaries encounter single adatoms. (Bottom) The mean square displacement Δx^2 of the boundary versus Δt for a range of adatom coverages from 0% to 60%. The inset shows one of the main mechanisms for pinning of the boundaries: a kink site decorated by an adatom in an off-lattice position.

a close-packed plane. In the course of a film's evolution, any of the sites in the lattice could become occupied at some point.

It is important that the rates for events in the KMC model are consistent with corresponding processes in the MD region. To ensure this, we simulated adatom diffusion in a purely MD system at temperatures up to $0.2\epsilon/k_B$. The result-

ing diffusion coefficient showed the usual Arrhenius dependence on temperature with an energy barrier of 0.29ϵ . This compares well with the barrier height estimated using the NEB method of 0.31ϵ . In addition, we were able to compute the prefactor for the KMC rate using the MD simulations which has a value of $0.38(m\sigma^2/\epsilon)^{1/2}$. The prefactor and energy barrier were then used to fix E_n and E_s . In addition, it is now possible for adatoms to diffuse across the MD-KMC boundary in either direction. A KMC atom that hops into the MD region is converted to a MD atom prior to the MD run beginning. However, a MD atom that leaves the MD region continues to undergo molecular dynamics until the next domain decomposition is performed. We note that KMC events continue to be chosen until the KMC clock exceeds 1τ .

We then simulated boundary movement using the synchronized hybrid method for a variety of adatom coverages. Figure 5 compares the displacement in time of a boundary at 2.5% adatom coverage with a boundary at 30% adatom coverage. Clearly, at 30% coverage, the boundary becomes pinned for long periods of time by adatom islands as indicated by the steps in the 30% trace. This effect is also summarized in Fig. 5, which shows Δx^2 vs Δt for a variety of adatom coverages. Also shown in the inset is one of the principle pinning mechanisms identified, where a kink site has become decorated by a diatomic island. Note that the pinning atom is in an off-lattice position, sitting in a fourfold hollow above the A gap, an effect which would not have been captured by our KMC simulation alone. Pinning of fcc-hcp boundaries by atoms in such fourfold hollow sites has recently been observed experimentally in homoepitaxial growth on Ir (111).⁷

Figure 5 also serves to illustrate the value of the hybrid scheme. First, with approximately 32% of the atoms remaining in the MD region in the runs used to collect the data shown here, the hybrid runs took $\sim 1/3$ of the time of a full MD run. Second, it can clearly be seen that the grain boundaries are leaving the initial MD region (width 30σ). In fact, in the trace shown at 30% adatom coverage, the boundary is pinned by a structure that has nucleated and grown *within* the

KMC region before the arrival of the boundary. In this way, the KMC does more than simply act as a static boundary condition for the MD, allowing the grain boundary the possibility of interacting with structures that form on spatial scales significantly larger than that of the MD domain w with a negligible increase in computational cost.

V. CONCLUSION

In conclusion, we have demonstrated an adaptive hybrid method that couples MD and KMC in a domain decomposition for dealing with inhomogeneities that develop in epitaxial growth. This method leads to a reduction in computational cost compared to conventional MD, reducing the execution time by a factor of approximately equal to the relative fraction of remaining MD atoms. We have shown that it is possible to reproduce grain boundary mobilities from full MD simulations with the domain decomposition method in the absence of KMC events. We have then used the method to study the effect of overlayer adatoms on the mobility of the boundaries, demonstrating that boundaries can become pinned by adatom islands. These effects would have been difficult to capture in a conventional KMC simulation. We expect that this method may be useful in other applications such as three-dimensional island growth or nanocluster coalescence and ripening. In addition, the domain decomposition could be extended to two and three dimensions rather than the simple one-dimensional decomposition used here. Furthermore, the method could also be used in conjunction with accelerated molecular dynamics methods.¹¹

ACKNOWLEDGMENTS

P.Z. and S.C.H. acknowledge the support from the New Zealand Foundation for Research, Science and Technology under Contract No. C08X0409. T.P.S. was supported by the U.S. DOE under Grant No. DE-FG02-03ER2558.

¹J. W. Evans, P. A. Thiel, and M. C. Bartelt, *Surf. Sci. Rep.* **61**, 1 (2006).

²T. Michely and J. Krug, *Islands, Mounds and Atoms* (Springer, Berlin, 2004).

³C. C. Battaile and D. J. Srolovitz, *Annu. Rev. Mater. Res.* **32**, 297 (2002).

⁴K. A. Fichthorn and M. Scheffler, *Phys. Rev. Lett.* **84**, 5371 (2000).

⁵C. Busse, C. Polop, M. Müller, K. Albe, U. Linke, and T. Michely, *Phys. Rev. Lett.* **91**, 056103 (2003).

⁶W. L. Ling, N. C. Bartelt, K. F. McCarty, and C. B. Carter, *Phys. Rev. Lett.* **95**, 166105 (2005).

⁷C. Busse and T. Michely, *Surf. Sci.* **552**, 281 (2004).

⁸J. de la Figuera, J. E. Prieto, C. Ocal, and R. Miranda, *Phys. Rev. B* **47**, 13043 (1993).

⁹S. Bleikamp, A. Thoma, C. Polop, G. Pirug, U. Linke, and T. Michely, *Phys. Rev. Lett.* **96**, 115503 (2006).

¹⁰J. de la Figuera, K. Pohl, O. Rodríguez de la Fuente, A. K. Schmid, N. C. Bartelt, C. B. Carter, and R. Q. Hwang, *Phys. Rev. Lett.* **86**, 3819 (2001).

¹¹A. F. Voter, F. Montalenti, and T. C. Germann, *Annu. Rev. Mater. Res.* **32**, 321 (2002).

¹²K. Hara, M. Ikeda, O. Ohtsuki, K. Terakura, M. Mikami, Y. Tago, and T. Oguchi, *Phys. Rev. B* **39**, 9476 (1989).

¹³G. Lu and E. Kaxiras, in *Handbook of Theoretical and Computational Nanotechnology*, edited by M. Rieth and W. Schommers (American Scientific, Stevenson Ranch, CA, 2006).

¹⁴A. B. Bortz, M. H. Kalos, and J. L. Lebowitz, *J. Comput. Phys.* **17**, 10 (1975).

¹⁵J. M. Pomeroy, J. Jacobsen, C. C. Hill, B. H. Cooper, and J. P.

- Sethna, Phys. Rev. B **66**, 235412 (2002).
- ¹⁶T. P. Schulze, P. Smereka, and W. E, J. Comput. Phys. **189**, 197 (2003).
- ¹⁷T. P. Schulze, J. Cryst. Growth **263**, 605 (2004).
- ¹⁸W. E and Z. Huang, Phys. Rev. Lett. **87**, 135501 (2001).
- ¹⁹A. C. To and S. Li, Phys. Rev. B **72**, 035414 (2005).
- ²⁰G. S. Grest and K. Kremer, Phys. Rev. A **33**, 3628 (1986).
- ²¹G. Mills, H. Jonsson, and G. K. Schenter, Surf. Sci. **324**, 305 (1995).
- ²²M. Müller, K. Albe, C. Busse, A. Thoma, and T. Michely, Phys. Rev. B **71**, 075407 (2005).
- ²³N. Combe, P. Jensen, and A. Pimpinelli, Phys. Rev. Lett. **85**, 110 (2000).